Geophys. J. Int. (2000) **143,** 113–118

Observation of Coriolis coupled modes below 1 mHz

W. Zürn,[1] G. Laske,[2] R. Widmer-Schnidrig[2] and F. Gilbert[2]

[1] *Black Forest Observatory, Heubach* 206, D-77709 *Wolfach, Germany. E-mail:walter.zuern@GPI.uni-karlsruhe.de*
[2] *Cecil and Ida Green Institute of Geophysics and Planetary Physics, UCSD, La Jolla,* CA 92093-0225, *USA*

Accepted 2000 May 3. Received 2000 March 20; in original form 1999 November 9

SUMMARY

We present observations of spectral energy at toroidal mode frequencies in vertical seismic recordings of the 1998 Balleny Islands earthquake. Since toroidal modes on a spherically symmetric, non-rotating Earth have horizontally polarized particle motion these observations call for an explanation. We first rule out local and instrumental effects as being responsible for the vertical-component signal of the toroidal modes ${}_0T_3$ (0.59 mHz) and ${}_0T_4$ (0.77 mHz). The global effects that we consider are general heterogeneous mantle structure, ellipticity of figure and rotation. We find that rotation through Coriolis coupling of low-order spheroidal and toroidal oscillations is the dominant mechanism.

Key words: Coriolis coupling, Earth's rotation, free oscillations.

1 INTRODUCTION

The spectrum of the Earth's seismic normal modes provides evidence for both its predominantly spherically symmetric internal structure and deviations from this idealized reference state. At frequencies below 1 mHz the most effective deviation from spherical symmetry is the Earth's diurnal rotation, which leads to Zeeman splitting of individual multiplets and to Coriolis coupling of pairs of nearby multiplets. Zeeman splitting of the lowest-order modes was first observed after the Great 1960 Chilean earthquake (Ness *et al.* 1961; Benioff *et al.* 1961) and subsequently Backus & Gilbert (1961) showed that the Earth's rotation removes the degeneracy of low-order normal nodes and leads to Zeeman splitting.

Coriolis coupling was shown to be ubiquitous between fundamental spheroidal and toroidal modes in the band 1.5–3.5 mHz (Masters *et al.* 1983). Coupling between multiplets leads to a perturbation of both their degenerate frequencies and their quality factors, and for many modes this perturbation of the degenerate frequency is more than 10 times larger than the observational uncertainty of the degenerate frequency. Hence the frequencies need to be corrected before such modes can be included in data sets for the construction of spherically symmetric elastic or anelastic earth models.

Towards lower frequencies the signal-to-noise ratio in seismic recordings rapidly decreases due to both increasing background noise levels and decreasing modal acceleration amplitudes (proportional to f^2). Fortunately, some of the noise is generated locally and is coherent with atmospheric pressure fluctuations such that the signal-to-noise ratio can be improved by a simple regression (Zürn & Widmer 1995). Applying this correction to vertical-component recordings of the recent Balleny Islands earthquake we find observational evidence for Coriolis coupling between spheroidal and toroidal modes below 1 mHz.

2 OBSERVATIONS

The great Balleny Islands earthquake (BIQ, M_w 8.2) of 1998 March 25 provided a new opportunity to study the low-frequency modes of the Earth. We investigated the records from several instruments at the Black Forest Observatory (BFO) after this earthquake in order to check the efficiency of the air pressure correction below 1.5 mHz for the different components. Zürn & Widmer (1995) were able to extract ${}_0S_2$ clearly from the noise in a vertical-component seismogram after the 1994 Shikotan earthquake using this correction. Inadvertently, this was also achieved by Virtanen (1996) from the record of a superconducting gravimeter at Metsähovi, Finland, as studies of long-period gravity variations routinely include this correction. The success of this correction is based on the fact that below 1.5 mHz a substantial part of the noise in vertical records is created by Newtonian attraction of the sensor mass and by vertical displacement of the surface due to atmospheric loading by the air masses above the station. We were again successful with the pressure correction and a 100 hr record from the gravimeter at BFO in the case of BIQ, albeit that for ${}_0S_2$ the signal-to-noise ratio (SNR) was not quite as good as for the Shikotan event and for a few other earthquakes (Zürn *et al.* 1999). Van Camp (1998, 1999) studied records of the BIQ from superconducting gravimeters in Membach (Belgium), Vienna (Austria) and Strasbourg (France) (Crossley *et al.* 1999) using the local pressure correction and obtained similar SNRs for low-order spheroidal modes.

However, close inspection of the spectra from the gravimeter unexpectedly reveals small but clear peaks at the frequencies of ${}_0T_3$, ${}_0T_4$ and ${}_0T_6$. Fig. 1 shows the spectra of 36-hr-long records of the LaCoste–Romberg gravimeter ET-19 at BFO after BIQ without and with application of the local pressure correction (with a regression coefficient of -3.75 nm s^{-2} hPa^{-1}). Both records show a clear peak at the frequency of ${}_0T_4$. For ${}_0T_3$ only the corrected spectrum shows a peak at the expected frequency, while the raw spectrum shows a small peak significantly offset to lower frequencies. Obviously the barometric effect significantly interferes with the seismic signal.

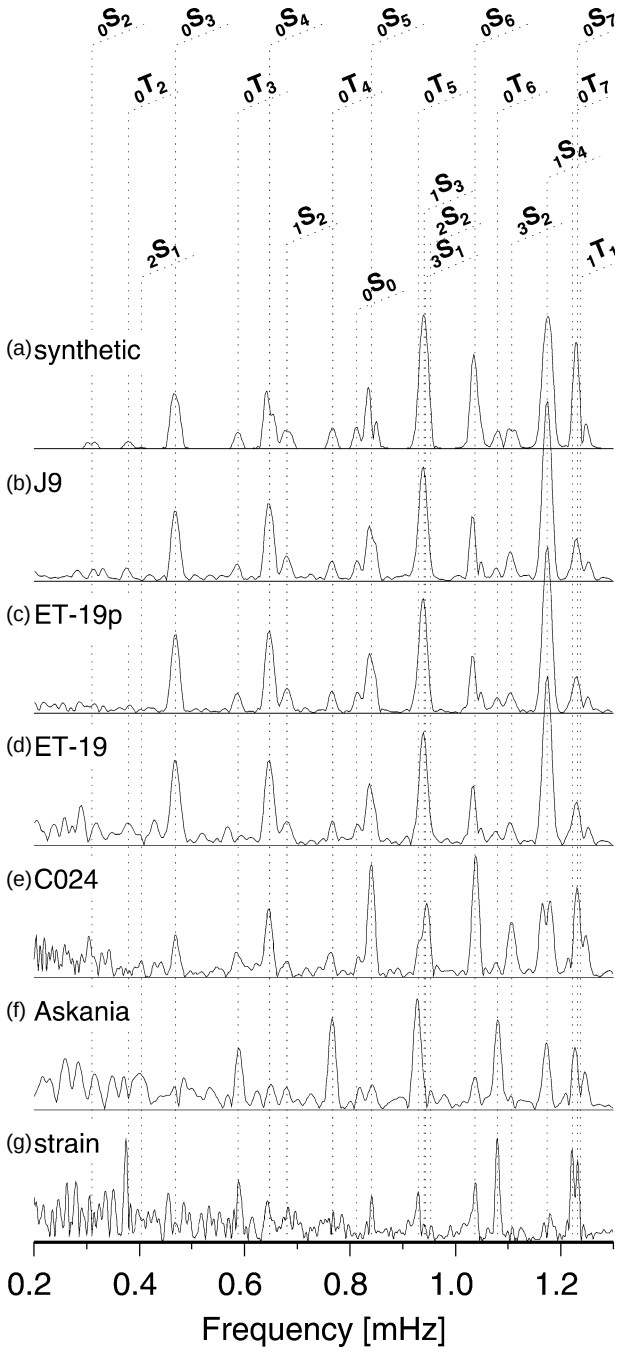

Figure 1. Comparison of amplitude spectra from the BIQ. The traces are (a) vertical-component coupled-mode synthetic for BFO including rotation, ellipticity of figure and heterogeneous elastic mantle structure, (b) C026 (J9, Strasbourg), pressure-corrected, (c) ET-19p (BFO), pressure-corrected, (d) ET-19 without pressure correction, (e) C024 (Boulder), pressure-corrected, (f) Askania N–S (BFO) and (g) shear strain N37.5°E (BFO). The lengths of the time-series (a)–(f) are 36 hr; that of (g) is 72 hr.

A close look at pressure-corrected spectra of records from three superconducting gravimeters published by Van Camp (1998, 1999) also reveals small peaks at these two frequencies. Fig. 1 shows the spectrum of the 36 hr record after BIQ from the superconducting gravimeter GWR-C026 at J9 near Strasbourg, about 60 km from BFO. The spectrum of a pressure-corrected record from the superconducting gravimeter GWR-C024 at Table Mountain Observatory near Boulder (CO, USA) also shows these peaks (Fig. 1), providing additional evidence for the global nature of this phenomenon.

The toroidal modes ${}_0T_3$ and ${}_0T_4$ are not clearly visible above the noise for all record lengths. Optimal SNR is obtained for $\sim$36 hr, which is only about half as long as the $1Q$ cycles recommended for frequency measurements (Dahlen 1982). While we accept these peaks as significant observations, their SNRs are not large enough to allow detailed investigation of their development with time. The initial amplitude of ${}_0T_3$ in the ET-19 record is estimated to be about 0.067 nm s^{-2} by spectral comparison with a decaying sinusoid of the proper eigenfrequency and a Q of 250. The same method is also used below for estimating the amplitudes of horizontal accelerations and strains.

We digress briefly to discuss the observations at BFO with horizontal components (Zürn *et al.* 1999). The following horizontal accelerometers recorded the BIQ at BFO: an upgraded Askania borehole tiltmeter, STS-1 seismometers and an STS-2 seismometer. The N–S components of all three types show SNRs of 3–5 for ${}_0T_3$–${}_0T_6$. The initial amplitude of the mode ${}_0T_3$ in the N–S components was roughly estimated to amount to about 1 nm s^{-2}, while ${}_0T_4$ was about 50 per cent larger. On the E–W components these two modes could not be detected in the noise, an observation from which an upper bound on the modal amplitudes may be placed. We find that E–W amplitudes must have been less than half the N–S amplitudes. A simple regression analysis using the local barometric record for the horizontal components did not improve the SNRs noticeably. The spectrum of a 36 hr record from the N–S component of the Askania tiltmeter is also shown in Fig. 1.

The strain meter array at BFO (Widmer *et al.* 1992) also recorded the BIQ, and we can identify the elusive mode ${}_0T_2$ in these records. The bottom trace in Fig. 1 shows a spectrum of a 72-hr-long Hanning tapered section after the BIQ for the combination of the three strain records that represents shear strain on a vertical plane with a strike of N37.5°E. For these instruments the SNR can also be improved by correcting for the local barometric pressure. The physical mechanism responsible for the success of the correction is likely to be pressure-induced local deformation of the ground (Zürn *et al.* 1999). Note that the amplitude of ${}_0T_3$ is less than that of ${}_0T_2$ and that ${}_0T_4$ is missing in this component of the deformation field at BFO, due to the proximity to a minimum in the strain field of ${}_0T_4$. We conclude that low-degree toroidal modes were excited very well by the BIQ and that at BFO horizontal accelerations were larger in the N–S than in the E–W components for the lowest-degree toroidal modes.

To quantify our observations further, we estimate multiplet frequencies by fitting synthetic resonance functions to

the spectra in Fig. 1. We obtain the following frequencies: $f[{}_0T_2]$ (374.7 ± 1.5) μHz, $f[{}_0T_3]$ (586.5 ± 2.0) μHz and $f[{}_0T_4]$ (765.0 ± 1.5) μHz. Note that these frequencies are not corrected for second-order effects due to rotation (Dahlen & Sailor 1979).

3 POSSIBLE MECHANISMS

What is the mechanism coupling these toroidal modes into the vertical component? First, we consider possible local and instrumental mechanisms because of the small number of sensors that show this new signal. These are the effects of the local heterogeneities (site effects, e.g. King *et al.* 1976), non-verticality of the sensitive direction of the sensor and electrical cross-talk from the horizontal components. Second, the Coriolis force acts on the sensor due to its motion in the E–W direction. Third, these modes could be globally coupled to nearby spheroidal modes by rotation, ellipticity, lateral heterogeneity or anisotropy. We first discuss the local possibilities.

3.1 Local effects

Local heterogeneities are very effective at modifying deformation fields, and therefore create complications in comparisons of observed and synthetic signals. The best known examples are observations of Earth tide tilts and strains, the interpretations of which are appreciably complicated by the local modifications of the signal. However, such effects have not so far been identified in records of tidal gravity, which places an upper bound on them. The mode strains of the BIQ at BFO are of the order of 10^{-11} at most, and the vertical displacement corresponding to the observed acceleration of ${}_0T_3$ (if interpreted as an inertial effect) is approximately 4 μm, thus coupling coefficients between strain and vertical displacement greater than 0.5 mm/10^{-9} would be needed to explain the observed vertical signal as an inertial effect. For tides such factors would produce 25 mm of vertical motion, which is at least 5 per cent of the tidal signal and this would definitely not have gone unnoticed at BFO and Strasbourg. We can thus rule out this effect.

The observed vertical acceleration would be produced by the N–S motion for ${}_0T_3$ if the sensitive direction of the gravimeters were off the local vertical by at least 3.5°. Tidal gravimeters are equipped with highly sensitive levels and thus much better aligned along the vertical than seismographs normally are. Such a misalignment would cause a contribution of at least 6 per cent to the vertical tide and again tidal work with the instruments would be noticeably affected, so we rule out this effect as well.

In order to explain the observed amplitudes on the vertical component with electrical cross-talk from some horizontal component, this effect would need to amount to 10 per cent. For the time of the BIQ this can be ruled out because large calibration pulses around this time did not cross-talk. Again, a problem of this magnitude would have been identified in tidal work.

Finally, by differencing the calibrated signals from BFO and Strasbourg (distance about 60 km) we found that both stations show the same amplitude and phase for the torsional modes on the vertical component. The three local effects considered are very unlikely to produce this property.

3.2 Coriolis force acting on the accelerometer

The vertical component of Coriolis acceleration for sinusoidal motion in the E–W direction with amplitude A_E and frequency f_0 at a station with colatitude θ is $b_C = 4\pi f_0 \sin(\theta) A_E \Omega$, where Ω is the angular velocity of the Earth (in rad s^{-1}). For mode ${}_0T_3$ at the latitude of BFO this value is $0.356 \times 10^{-6}\ A_E$ (s^{-2}). For ${}_0T_4$ the vertical acceleration is about 30 per cent higher. The ratio of these rotational accelerations in the vertical to the inertial acceleration in the E–W direction is given by $r = \sin(\theta)\Omega/(f_0\pi)$. For BFO and Strasbourg this ratio is roughly 1/400. Note that N–S motion does not produce vertical accelerations. Combining our upper bound on the E–W amplitudes and our amplitude estimate of vertical acceleration, the signals in the vertical are then at least a factor of 80 too high in order to be explained by these effects. The multiplet character of the modes somewhat complicates the problem; therefore, we resort to synthetic seismograms.

In order to represent the response of an idealized accelerometer we use an effective acceleration (Dahlen & Tromp 1998, Section 4.4). The effective acceleration takes into account small perturbations in gravity, caused by the motion, as well as tilt (Dahlen & Tromp 1998, eq. 4.183). At very low frequencies it is important to take into account the effects of rotation (Dahlen & Tromp 1998, eq. 4.184). Explicitly, the effective acceleration or forcing term, F, for the indicator equation for an idealized accelerometer is as follows.
Vertical polarization, $\hat{r}$:

$$F = \omega^2 U - \partial_r \Phi - 4\pi G\rho U + 2a^{-1} g U - 2i\omega\Omega(\partial_\phi V - \sin\theta\, \partial_\theta W)\,; \tag{1}$$

horizontal polarization, $\hat{h}$:

$$F = \hat{h}(\omega^2[\nabla_1 V - \hat{r}\times\nabla_1 W] - a^{-1}[\nabla_1\Phi + g\nabla_1 U] - 2i\omega\Omega[\cos\theta\ \hat{r}\times\nabla_1 V + \sin\theta\,\hat{\phi}U + \cos\theta\,\nabla_1 W])\,. \tag{2}$$

Terms of order Ω^2 have been omitted. The remaining symbols have their usual meanings.

Since the acceleration due to the Coriolis force is proportional to Ω/ω, where ω is the frequency of the signal, we expect accelerations on the vertical component of 1.2 and 2 per cent of the E–W acceleration at the frequencies of ${}_0T_4$ and ${}_0T_3$, respectively. This expectation was confirmed by a set of synthetic seismograms and thus the local effect of the Coriolis force can be ruled out as being responsible for our observations of ${}_0T_3$ and ${}_0T_4$ in vertical seismic recordings.

It is noteworthy that the Coriolis force on the accelerometer can generate Love wave signals on vertical components with amplitudes reaching 0.1–1 per cent of the signal on the E–W component. This effect is most likely to be observationally relevant during the passage of large-amplitude Love waves propagating on a near-polar path. Love wave signals in vertical-component recordings (so-called quasi-Love waves) have indeed been observed and have been invoked as evidence for seismic anisotropy in the upper mantle (e.g. Park 1986; Park & Yu 1992). Although our effect is smaller than the reported signal of these authors, the possibility remains that the Coriolis force on the accelerometer mimics the effect of weak seismic anisotropy.

3.3 Coupling due to rotation, ellipticity and 3-D structure

We must turn to global coupling of toroidal and spheroidal modes to explain our observation. It is well known since the work of Masters *et al.* (1983) that peaks at toroidal mode frequencies can be found in vertical accelerometer records at higher frequencies due to Coriolis coupling with spheroidal modes. This coupling is especially strong where the frequency of a toroidal mode is close to the frequency of a spheroidal mode and their respective harmonic degrees differ by one. The strongest coupling observed so far was thus for the pair ${}_0T_{11}$–${}_0S_{10}$. Modes below 1 mHz have a much larger spacing in the frequency domain and therefore coupling was not recognized in this range, even though theory predicts it, as we discuss below.

We briefly review variational theory for multiplet coupling on a rotating, elliptical, anelastic and heterogeneous earth (Woodhouse & Dahlen 1978; Dahlen & Sailor 1979; Woodhouse 1980; Dahlen & Tromp 1998) and identify coupling mechanisms that could explain our observations. The calculations of mode splitting due to the Earth's rotation (rotational coupling) usually include first- and second-order terms in Ω/ω_0 (Ω is the sidereal rotation rate and ω_0 the fiducial frequency of a mode) caused by the Coriolis force and the second-order terms caused by the centrifugal force (e.g. Dahlen & Sailor 1979). Coupling due to the ellipticity of the Earth is a second-order term. The coupling between multiplets is governed by a set of angular-degree selection rules (below we give a summary of Woodhouse 1980 and Dahlen & Tromp 1998):

(i) the Coriolis force causes spheroidal–toroidal mode coupling of mode pairs of the form ${}_nS_{\ell-n'}T_{\ell\pm1}$, that is, between multiplets that differ by a single angular degree ($|\ell-\ell'|=1$, e.g. ${}_0S_4$–${}_0T_3$, ${}_0S_5$–${}_0T_4$, ${}_1S_4$–${}_0T_3$);
(ii) the ellipticity of the Earth also causes spheroidal–toroidal mode coupling for $|\ell-\ell'|=1$;
(iii) rotation causes spheroidal–spheroidal coupling for $|\ell-\ell'|=0$;
(iv) ellipticity causes same-type (spheroidal or toroidal) mode coupling for $|\ell-\ell'|=0$ and for $|\ell-\ell'|=2$.

Only spheroidal–toroidal mode coupling generates vertical motion at toroidal mode frequencies, so rules (iii) and (iv) are irrelevant for the observations discussed here.

We also consider the effects of 3-D structure. Lateral heterogeneity of harmonic degree s causes spheroidal–toroidal mode coupling under the conditions that $|\ell'-\ell|+1\le s\le\ell'+\ell-1$ and $\ell'+\ell+s$ is odd. Hence, the mode pair ${}_0S_4-{}_0T_3$ is coupled through structure of degrees 2, 4 and 6. Note that modes couple through structure of odd harmonic degree if $|\ell-\ell'|$ is even (e.g. ${}_0S_5$ couples to ${}_0T_3$ through $s=3$, 5 and 7) and that ellipticity of figure is just a special case of a heterogeneous structure with $s=2$.

To illustrate the effect of spheroidal–toroidal mode coupling we compare synthetic seismograms that are calculated using the coupled-mode code of Park & Gilbert (1986). Rotation of the Earth, ellipticity and aspherical elastic mantle model S16B30 (Masters *et al.* 1996), but no 3-D attenuation, are included in the calculations. All spheroidal, toroidal and radial modes up to 1.6 mHz are included in the coupling calculations and we use elastic 1-D model 1066A (Gilbert & Dziewonski 1975) to calculate eigenfunctions. The 1-D attenuation model is QL6 (Durek & Ekström 1989). The synthetic spectra of Fig. 2 clearly indicate that rotational coupling is the most effective mechanism for generating toroidal mode energy on the vertical component. Spheroidal–toroidal mode coupling due to ellipticity accounts for less than 10 per cent of the toroidal mode signal on the vertical. We also find that for modes below 1 mHz, coupling due to aspherical mantle structure (S16B30) is even weaker than coupling due to ellipticity.

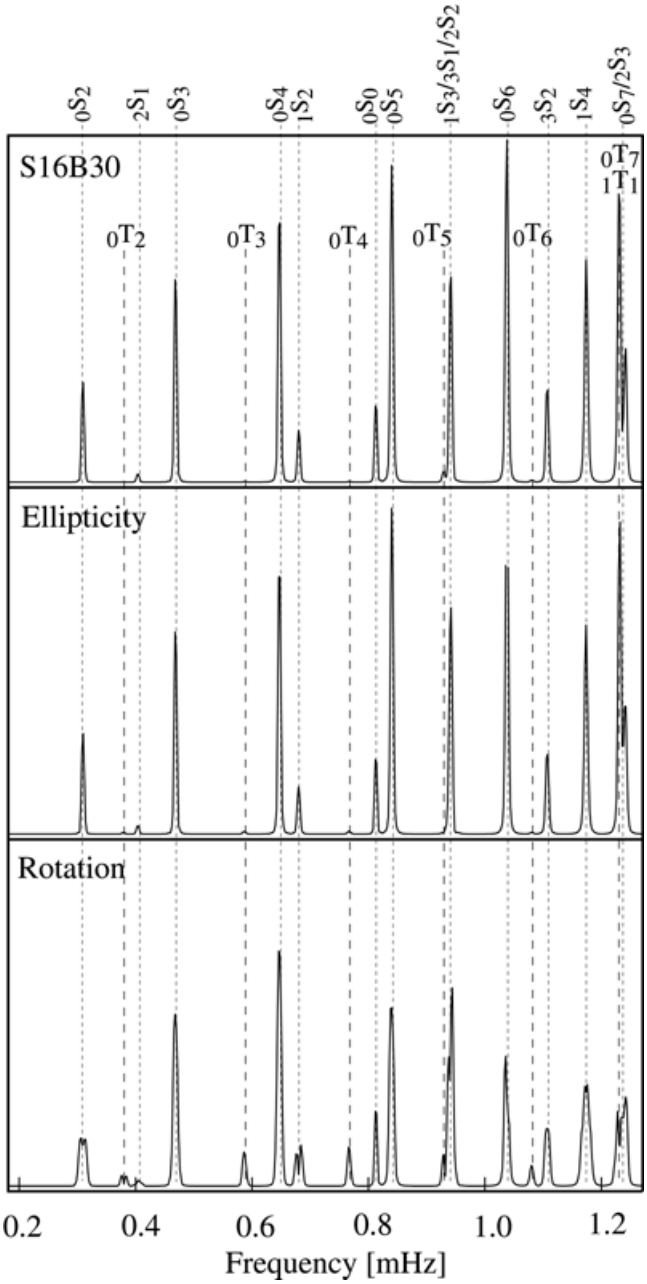

Figure 2. Spectra of 100-hr-long coupled-mode vertical-component accelerograms computed for the BIQ and station BFO. Modal excitations are computed based on the Harvard centroid moment tensor. In the top panel, only 3-D mantle model S16B30 (Masters *et al.* 1996) was used in the coupling calculations, while the middle panel used only ellipticity and the bottom panel only the rotation of the Earth. Clearly, rotation is the most effective mechanism for peaks to appear at toroidal mode frequencies.

Since amplitude effects of the spectral peaks at a particular station may be poor indicators for the coupling strength between modes, we have also determined the multiplet frequency shifts for the three coupling mechanisms (Table 1). Multiplet frequencies are computed as arithmetic means of the hybrid singlet frequencies. Rotational effects are obviously the dominant effects for the low-ℓ toroidal modes (${}_0T_2 - {}_0T_6$). Note that the effects on ${}_0T_5$ are difficult to assess in Fig. 2 as ${}_0T_5$ significantly overlaps with the spheroidal mode cluster ${}_1S_3/{}_3S_1/{}_2S_2$. Our results for rotational coupling may differ slightly from the shifts obtained in Dahlen & Sailor (1979) as we use a different attenuation model and do not include absolutely all modes that can couple. In particular, our calculations account only for the coupling of up to seven nearest neighbours and our catalogue of modes does not include inner core toroidal modes, the Slichter mode ${}_1S_1$ and the nine secular modes of degree $\ell = 1$ that correspond to rigid body rotation of the mantle and inner core and rigid translation of the Earth as a whole.

We also linearize the quadratic eigenvalue problem for the frequencies in a coupling block (Park & Gilbert 1986, eq. 26) by choosing a fiducial frequency, $\hat{\omega}_0$, and combining the two interaction matrices **V** and **W** (Park & Gilbert 1986, eq. 39). Park (1985) has shown that the linear eigenvalue formulation wrongly predicts the sign of the second-order Coriolis interaction for a few grave, low-order multiplets (${}_0S_2$, ${}_0S_3$, ${}_2S_1$, ${}_0S_4$, ${}_1S_2$, ${}_1S_3$, ${}_1S_4$, ${}_0T_2$, ${}_1T_1$). This leads to a small bias in the fiducial frequency of these modes, while the splitting width remains practically unaffected. Choosing the linear over the quadratic approach leads to a shift in the fiducial frequency for ${}_0S_2$ of 0.25 μHz when coupled to ${}_0T_3$ (Table 1 of Park & Gilbert 1986). We expect a similar bias for ${}_0T_2$. Since the predicted multiplet frequency shifts in Table 1 are smaller than our observational uncertainties, we do not pursue the cause of the discrepancies between the Dahlen & Sailor (1979) values and ours any further. We merely want to stress that mode coupling due to rotation dominates at frequencies below 1 mHz over coupling due to ellipticity or heterogeneous mantle structure.

4 DISCUSSION

When compared with the observationally well-established Coriolis coupling between fundamental spheroidal and toroidal modes in the band 1.5–3.5 mHz (Masters *et al.* 1983), we note that below 1 mHz frequency coupling appears to be relatively weak while amplitude coupling appears to be strong. In other words, multiplet degenerate frequencies and quality factors are barely affected while hybrid singlet eigenfunctions appear to have large components of their respective coupling partners.

Note that if the splitting matrix for Coriolis-coupled spheroidal and toroidal modes can be observed, then the Coriolis terms are linear constraints on the radial distribution of density (Dahlen & Tromp 1998, eq. D.68).

Table 1. Shift of the fiducial frequencies of the first six fundamental toroidal modes due to rotation, ellipticity and 3-D mantle structure (S16B30, see text for details) in the presence of mode coupling (first and second order in Ω/ω). Frequency shifts are given in μHz. For comparison, the values for mode ${}_0T_{19}$ are also given.

Mode	D&S[1]	Rotation	Ellipticity	S16B30
${}_0T_2$	−0.684	−0.834	−0.008	−0.004
${}_0T_3$	−0.328	−0.438	−0.003	−0.007
${}_0T_4$	−0.180	−0.266	−0.003	−0.010
${}_0T_5$	−0.099	−0.171	0.000	−0.026
${}_0T_6$	−0.052	−0.074	0.002	−0.013
${}_0T_7$	−0.012	−0.007	0.003	+0.003
${}_0T_{19}$	–	−3.401	0.000	−0.018

[1] Frequency shifts due to rotation given by Dahlen & Sailor (1979)

ACKNOWLEDGMENTS

We would like to thank Jacques Hinderer for the data from Strasbourg and Tonie van Dam for the data from Boulder. We also thank Michel Van Camp for sending us a copy of his thesis and a preprint. Special thanks go to Guy Masters for numerous helpful discussions and the mode-coupling code. A very insightful and constructive review was provided by Jeffrey Park. Thanks also go to Jeroen Tromp, who provided the second review of this manuscript. This research was financed by National Science Foundation grant EAR-97-06056.

REFERENCES

Backus, G. & Gilbert, J., 1961. The rotational splitting of the free oscillations of the earth, *Proc. Nat. Acad. Sci.,* **47,** 362–371.

Benioff, H., Press, F. & Smith, S., 1961. Excitation of the free oscillations of the earth by earthquakes, *J. geophys. Res.,* **66,** 605–619.

Crossley, D. *et al.*, 1999. Network of superconducting gravimeters benefits a number of disciplines, *EOS, Trans. Am. geophys. Un.,* **80,** 121, 125–126.

Dahlen, F., 1982. The effect of data windows on the estimation of free oscillation parameters, *Geophys. J. R. astr. Soc.,* **69,** 537–549.

Dahlen, F. & Sailor, R., 1979. Rotational and elliptical splitting of the free oscillations of the earth, *Geophys. J. R. astr. Soc.,* **58,** 609–623.

Dahlen, F. & Tromp, J., 1998. *Theoretical Global Seismology,* Princeton University Press, Princeton, NJ.

Durek, J. & Ekström, G., 1989. A model of radial anelasticity consistent with observed surface wave attenuation, *Bull. seism. Soc. Am.,* **86,** 144–158.

Gilbert, F. & Dziewonski, A., 1975. An application of normal mode theory to the retrieval of structural parameters and source mechanisms from seismic spectra, *Phil. Trans. R. Soc. Lond.,* **A278,** 187–269

King, G.C.P., Zürn, W., Evans, R. & Emter, D., 1976. Site correction for long-period seismometers, tiltmeters and strainmeters, *Geophys. J. R. astr. Soc.,* **44,** 405–411.

Masters, G., Park, J. & Gilbert, F., 1983. Observations of coupled spheroidal and toroidal modes, *J. geophys. Res.,* **88,** 10 285–10 298.

Masters, G., Johnson, S., Laske, G. & Bolton, H., 1996. A shear velocity model of the mantle, *Phil. Trans. R. Soc. Lond.,* **A354,** 1385–1411.

Ness, N., Harrison, C. & Slichter, L., 1961. Observations of the free oscillations of the earth, *J. geophys. Res.,* **66,** 621–629.

Park, J., 1985. Applications of the Galerkin formalism in the coupling of the earth's free oscillations, *PhD thesis,* University of California, San Diego, La Jolla.

Park, J., 1986. Synthetic seismograms from coupled free oscillations: the effects of lateral structure and rotation, *J. geophys. Res.,* **91,** 6441–6464.

Park, J. & Gilbert, F., 1986. Coupled free oscillations of an aspherical dissipative rotating earth: Galerkin theory, *J. geophys. Res.,* **91,** 7241–7260.

Park, J. & Yu, Y., 1992. Anisotropy and coupled free oscillations: simplified models and surface wave observations, *Geophys. J. Int.,* **110,** 401–420.

Van Camp, M., 1998. Qualification d'un gravimètre cryogénique pour les périodes supérieures à cent secondes, *Thèse du Doctorat,* Université Catholique de Louvain, France.

Van Camp, M., 1999. Measuring seismic normal modes with the GWR C021 superconducting gravimeter, *Phys. Earth planet. Inter.,* **116,** 81–92.

Virtanen, H., 1996. Observation of free oscillations of the earth by superconducting gravimeter GWR T-020, *Acta Geod. Geophys. Hung.,* **31,** 423–431.

Widmer, R., Zürn, W. & Masters, G., 1992. Observation of low order toroidal modes from the 1989 Macquarie rise event, *Geophys. J. Int.,* **111,** 226–236.

Woodhouse, J., 1980. The coupling and attenuation of nearly resonant multiplets in the earth's free oscillation spectrum, *Geophys. J. R. astr. Soc.,* **61,** 261–283.

Woodhouse, J. & Dahlen, F., 1978. The effect of a general aspherical perturbation on the free oscillations of the earth, *Geophys. J. R. astr. Soc.,* **53,** 335–354.

Zürn, W. & Widmer, R., 1995. On noise reduction in vertical seismic records below 2 mHz using local barometric pressure, *Geophys. Res. Lett.,* **22,** 3537–3540.

Zürn, W., Widmer-Schnidrig, R. & Bourguignon, S., 1999. Efficiency of air pressure corrections in the BFO records of the Balleny Islands earthquake, March 25, 1998, *Bull. Info. Marées Terrestres,* **131,** 10 183–10 194.